A Tetherless, Absolute-Time Channel Sounder; Processing and Results for a Complex Environment*

David Novotny[1], Alexandra Curtin[2], Jeanne Quimby[2], Kate Remley[2], Peter Papazian[2], Richard Candell[3]

[1] National Institute of Standards and Technology: Communications Technology Laboratory, Boulder, CO, USA, david.novotny@nist.gov

[2] National Institute of Standards and Technology: Communications Technology Laboratory, Boulder, CO, USA

[3] National Institute of Standards and Technology: Engineering Laboratory, Gaithersburg, MD, USA

***Abstract*— We present a channel sounder that can operate without a tether and still maintain an absolute time reference between the source and receiver. Based on a sliding correlator, with synchronized rubidium clocks to generate phase references for the up- and down- converted RF carriers, and a synchronous trigger, the system generates locked signals in the short term (tens of hours). The system has an operational range of 10 MHz to 6 GHz with an instantaneous channel bandwidth of up to 200 MHz.**

We start with a discussion on processing measurements for oversampled band-limited signals. Spectral truncation is compared with transmit spectrum filtering; DC bias removal and referencing to remove systematic effects are discussed.

We conclude with channel sounding results, power delay profile, RMS delay spread, and time of arrival versus position for an electromagnetically complex environment.

***Index Terms*— channel sounding, propagation, power delay profile, impulse response.**

I. Introduction

The realized propagation path between two points can vary greatly from Friis transmission in non-free-space environments. Basic free space loss [1] does not adequately explain the multi-path and lossy environments seen by modern communications systems. The ability to estimate the propagation characteristics between multiple points impacts radio channel quality, radio system capacity and thus radio system design and, more importantly, cost.

Many channel sounders have been built over different frequency ranges [2-11]. They have used single frequency, wideband noise and patterns that emulate protocol and data load to sound the channel. One major hurdle is that the propagation channel is not static, but can change rapidly and vary greatly in loss and dispersion. Characterizing many environments to get the spread of the data and losses is an arduous task. Comparing data from many measurements using different methods is difficult. The decision on what data to use, what scenarios need to be addressed, and how to cover the greatest range of realistic propagation environments is diffcult.

Many sounding analyses report the channel (TX antenna, propagation environment and RX antenna) convolved with a transmit spectrum of the sounder. To use the sounding results for a general transmit spectrum, the original transmit spectrum can be removed and the desired transmit spectrum can be re-applied. We propose a slightly different method for data reporting. By reporting only a channel response to frequencies with high signal to noise ratio (SNR), the response through a system can be estimated by convolving the reported response with an arbitrary transmit sequence.

We present a tetherless absolute-time channel sounder and methods for processing the results to represent the response of a specific data channel with limited dependence on the transmit spectrum of the sounder. These measurements were done in manufacturing facilities to help investigate the penetration of wireless networking signals in a very multi-path rich environment. Data were taken at three manufacturing facilities near two Industrial, Medical and Scientific (ISM) bands at 2.45 and 5.8 GHz. This paper only addresses part of the data; however, all of the data taken are available to independent third parties to perform comparative analysis [12].

II. System Methodology

Two major design decisions drove the overall architecture of our channel sounder: tetherless operation and absolute time referencing. Tetherless operation allows not only for large physical distance variations, but the ability to measure complex operational environments with minimal disturbance to the environment itself. The absolute time reference provides detailed delay information for the channel. The ability to measure absolute delay without Global Positioning Systems (GPS) allows for accurate channel measurements in cluttered and shadowed areas. The single step referencing performed here does require physical connection between the source and receiver but in return, it removes all (non-channel) linear systematic delays and losses.

A. System Architecture

Fig. 1 shows an overall block diagram of the system. A recurring, oversampled pseudorandom (PN) code word is triggered repetitively and transmitted through an amplifier and a matched filter to limit radiated harmonics. The amplified signal is sampled to determine the actual power transmitted. Finally the signal is routed through an attenuator for referencing or the antennas to determine a complex impulse response (CIR) or power delay profile (PDP).

Two stable and independent timing chains maintain synchronization between the separated transmitter and receiver. Trigger timing and the radio frequency (RF) up- and down-conversion must be locked and synchronized. Rubidium (Rb) clocks have been used extensively in the channel sounding community to synchronize local oscillators (LO) for frequency conversion [10-11]. We use these clocks in the frequency conversion process. Additionally, a synchronized timing reference is generated with the pulse per-second (PPS) output from the clock. This Rb-sourced PPS signal is divided by the synchronization hardware to create a reference trigger to coherently initiate signal generation and acquisition. The redundancy of 10 MHz signals to the triggering and frequency conversion sections of the system (see Fig. 2) limits the amount of distribution jitter to minimize phase and time drift.

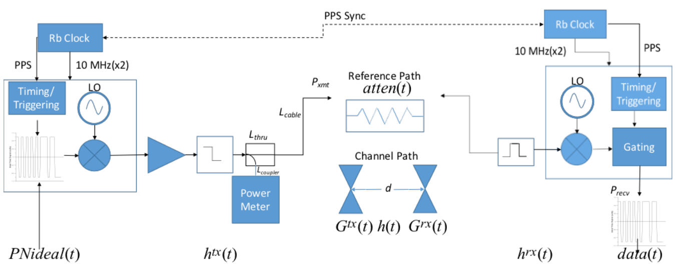

Figure 1. System architecture of the channel sounder. Measuring through the reference attenuator generates a known loss and delay reference that can be compared to the channel data through the antennas and propagation path to determine the channel complex impulse response.

B. Calibration Steps

- Transmit losses L_{thru}, $L_{coupler}$, L_{cable}, $L_{attenuator}$ are measured to allow for accurate calculation of the actual transmitted power and reference loss.
- Vector signal transceiver (VST) is power calibrated and referenced against an external power meter.
- PPS is linked between Rb clocks and allowed to stabilize.
- PPS is reestablished between the transmitter and receiver. Each chassis is disciplined to the PPS from its clock. This creates an accurate timing frame between the two chassis with the nominal stability of the clocks ($1\text{x}10^{-11}$ sec/100 sec).
- A synchronized trigger is generated relative to the PPS.
- A reference measurement is taken through the attenuator to establish delay and loss between the chassis.

III. Calculations of Channel Impulse Response and Power Delay Profile.

A. Removal of Systematic Components.

From Fig. 1, the output data, *data(t)*, is the input PN code word, $PN_{ideal}(t)$, transmitted through the transmitting system, $h^{tx}(t)$, the channel represented by the transmitting antenna, $G^{tx}(t)$, the environment, $h(t)$, and the receiving antenna, $G^{rx}(t)$, and finally the receiving system, $h^{rx}(t)$. During the reference calibration, the channel, $G^{tx}(t)*h(t)*G^{rx}(t)$, is replaced by an attenuator, *atten(t)*, so the systematic effects of the measurement system can be minimized.

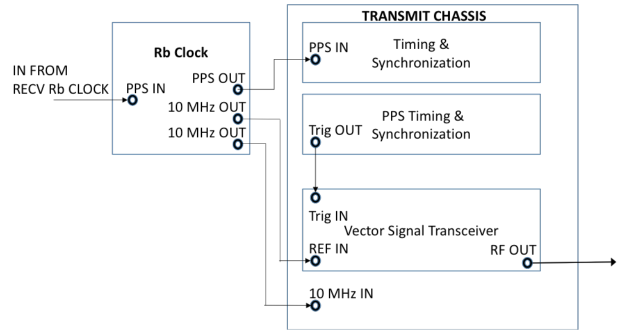

Figure 2. Timing and synchronization connections for the channel sounder. The multiple connections between the clock and chassis limit 10 MHz propagation errors between chassis components. The 10 MHz reference to the chassis provides inter-function synchronization while the 10 MHz to the transceiver provides a reference for frequency conversion. The receive chassis mirrors this setup.

The received data can be expressed equivalently in the time and frequency domains:

$$
\begin{aligned}
&data(t) = PN_{ideal}(t) * h^{tx}(t) * G^{tx}(t) * h(t) * G^{rx}(t) * h^{rx}(t), \\
&\boldsymbol{data}(f) = \mathcal{F}(data(t)) = \\
&\boldsymbol{PN}_{ideal}(f) \cdot \boldsymbol{h}^{tx}(f) \cdot \boldsymbol{G}^{tx}(f) \cdot \boldsymbol{h}(f) \cdot \boldsymbol{G}^{rx}(f) \cdot \boldsymbol{h}^{rx}(f),
\end{aligned}
\tag{1}
$$

where $\mathcal{F}$ denotes the Fourier transform, the "*" operator denotes convolution in the time domain, and the "•" operator denotes frequency-by-frequency multiplication. The channel's desired complex impulse response, *CIR(t)*, is given by just the radiated portion of the measurement:

$$CIR(t) = G^{tx}(t) * h(t) * G^{rx}(t). \tag{2}$$

A reference measurement is taken through a known attenuator. The resultant measurement yields a nominal characterization of the measurement system without the channel:

$$
\begin{aligned}
&ref(t) = PN_{ideal}(t) * h^{tx}(t) * atten(t) * h^{rx}(t), \\
&\boldsymbol{ref}(f) = \mathcal{F}(ref(t)) = \boldsymbol{PN}_{ideal}(f) \cdot \boldsymbol{h}^{tx}(f) \cdot \boldsymbol{atten}(f) \cdot \boldsymbol{h}^{rx}(f).
\end{aligned}
\tag{3}
$$

Assuming the system is linear with received power and time stable, this allows for a normalization of the measurement by the reference to yield *CIR(f)*:

$$
\begin{aligned}
&\frac{\boldsymbol{data}(f)}{\boldsymbol{ref}(f)} = \\
&\frac{\boldsymbol{PN}_{ideal}(f) \cdot \boldsymbol{h}^{tx}(f) \cdot \boldsymbol{G}^{tx}(f) \cdot \boldsymbol{h}(f) \cdot \boldsymbol{G}^{rx}(f) \cdot \boldsymbol{h}^{rx}(f)}{\boldsymbol{PN}_{ideal}(f) \cdot \boldsymbol{h}^{tx}(f) \cdot \boldsymbol{atten}(f) \cdot \boldsymbol{h}^{rx}(f)} = \\
&\frac{\boldsymbol{CIR}(f)}{\boldsymbol{atten}(f)}.
\end{aligned}
\tag{4}
$$

This can be rewritten into the time domain:

$$CIR(t) = \mathcal{F}^{-1}\left[\boldsymbol{CIR}(f)\right] = \mathcal{F}^{-1}\left[\frac{\mathcal{F}\left[data(t)\right]}{\mathcal{F}\left[ref(t)\right]} \cdot \boldsymbol{atten}(f)\right]. \tag{5}$$

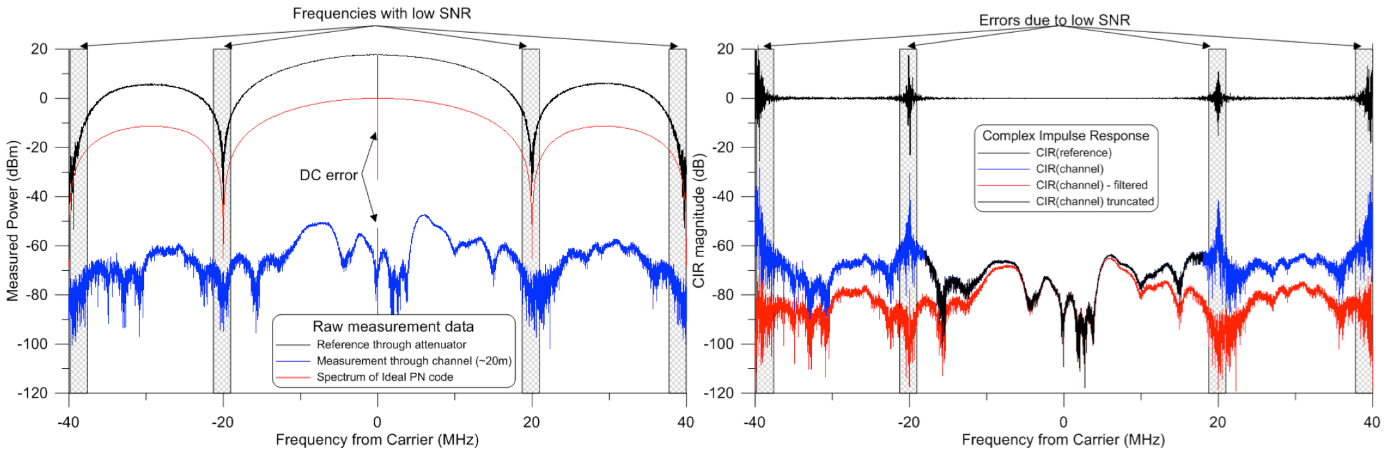

Figure 3. Spectrum of the reference and a measurement (left) and the CIR of the reference and measurement (right) show the effects of reference normalization and filtering options. DC bias removal, filtering, and proper truncation limit transitions that raise the noise floor in the PDP.

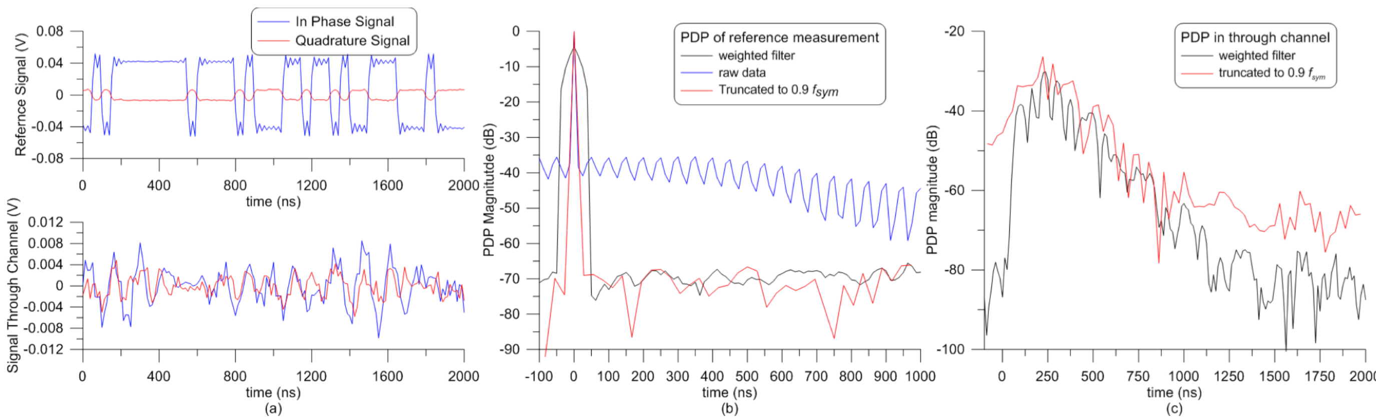

Figure 4. (a) Raw time-domain reference and measurement signals; tracking the I/Q phase provides Doppler information for rapidly changing channels. The PDP of the reference (b) shows the desired impulse at zero time, the unfiltered, raw data shows ringing due to the errors shown in Fig.3. Truncation (c) has a larger time step and the step at the end of the frequency record does show a higher noise floor than the weighted filter.

Note that the *atten(f)* is the transmission coefficient of the attenuator, so a frequency invariant 50 dB attenuator will have $atten(t) = atten(f) = 10^{-50/20} \approx 0.00316$.

B. Systematic Error Due to DC Biasing.

DC sampling errors can come from two sources: down-conversion errors and sampler offsets. The down-conversion errors primarily arise from small frequency errors between the transmitter and receiver, and from mixer leakage. At low signal levels, the DC bias in the sampler may be a significant source of error especially once transformed back to the time domain. The net DC error is often seen as a transition right at the carrier frequency or zero frequency in the down converted spectrum, (see Fig. 3). Practically, DC can't be transmitted over the air, and the DC error is compressed into one frequency component. Finally, the frequency components in the measurements are correlated through the FFT. A simple correction for fixing the DC error can be performed through a complex average of the points on either side of the DC term [13]:

$$CIR(0) = \frac{CIR(\Delta f) + CIR(-\Delta f)}{2}. \qquad (6)$$

The PDP can be generated from the corrected *CIR(t)*:

$$PDP(t) = \left|CIR(t)\right|^2. \qquad (7)$$

C. Addressing Spectral Power, Noise and Over Sampling.

The calculations of the CIR and PDP in (6) and (7) require a division by the spectrum of the reference through the attenuator. A transmitter has a limited bandwidth (limited by allowable TX power, regulation, or frequency of interest). Further, in order to improve dynamic range performance, the received signal is often oversampled in time to improve correlation results. This oversampling extends the effective measured frequency range. However, frequencies above the symbol frequency lack spectral power. This results in some measured frequencies with little transmitted power resulting in the noise/noise issue in (5), see Fig. 3. While using a BPSK PN code offers considerable processing gain, it lacks spectral strength above the symbol frequency f_{sym}. Other modulations and filters (matched cosine) can be used, but all over-sampled time-domain based systems will suffer low SNR over some portion of the measured frequency spectrum.

1) Filtering the Complex Impulse Response.

A common method to normalize energy lost to the filtering process is to correct for the energy of the applied filter [14]. This filtering creates an effective CIR:

$$CIR_{eff}(t) = w'(t) * CIR(t) = \frac{w(t)}{\sqrt{\int_t w(t)\,dt}} * CIR(t). \qquad (8)$$

Various filters can be used for *w(t)*; the primary requirement is to have a frequency zero at the symbol frequency. Brick-wall filters can be effective, but may introduce time-domain ringing. A common implementation is to use the ideal spectral power of the transmitted signal (see Fig. 3) as the filter, *w(t)*. This filter has an ideal zero power null that coincides with the nulls in the transmit spectrum. It does reduce the peak level of the ideal impulse and spreads it out in time. This can result in the measured path loss and the root mean square (RMS) delay spread, both critical communications parameters, being a function of the applied filter versus a physical characteristic of the channel itself.

2) Frequency Truncation of Complex Impulse Response.
Another filtering approach is to truncate the frequency range of the measurement to the frequencies with high SNR. This is different than applying a brick wall filter. In this case, the out of band components are removed, not zero filled. This limits the change in the PDP due to signal processing while maintaining the processing gain of the long over-sampled sequence, but at the price of reduced effective sampling and temporal resolution in the final PDP.

A suggested frequency truncation window is to limit the frequency extent of the CIR to where the transmitted signal drops below a given level. For a *sin(f)/f* spectrum of a PN code, the -20 dB level correlates to approximately ±0.9 f_{sym}, and -30 dB uses approximately ±0.97 f_{sym}. Practically, the filtering methods used in [13-15] limit the utilized spectrum to approximately the 20 to 30 dB SNR level, but a truncation approach reduces variability due to the chosen filter.

3) Comparitive Discussions of Filtering.
Truncation limits the reported frequency coverage and time-domain resolution. However, it reports lower uncertainties in the declared frequency channel. For this case of a 20-MHz symbol rate, a ±20-MHz or 40-MHz channel response is often reported. However, the uncertainty is higher near the band edges. Truncating to the -20 dB level, in this case ±18 MHz or 36 MHz, returns results with smaller noise related uncertainties in the reported band, however Fig. 4 also shows the potential for a higher noise floor and possibly less dynamic range due to reducing the processing gain from lower oversampling.

Optimizations can be made; using root-raised-cosine pulse shaping can flatten the transmitted spectrum and limit nulls. However, oversampling will still result in frequency regions of little power. Post-normalization filtering or truncation is needed to reduce the frequencies to bands of interest.

IV. Channel PDP Data From Two Manufacturing Environments.

The purpose of channel sounders is to measure how signals propagate in real environments. Measurements using the channel sounder described here were performed at two different factory environments. These measurements were focused on determining optimal placement of wireless IEEE 802.11 infrastructure, as well as the basic operational validity of the sounder. To emulate the propagation characteristics of the 802.11 bands, but yet not interfere with nearby installed systems, tests were performed in government bands at 2.245 GHz and 5.4 GHz. Table I shows the measurement parameters used. While all the data are available online for multiple facilities, we present data for one transmitter position (TX1) and two receiver polarizations at 2.245 GHz. We present a CIR, PDP, and RMS delay spread for a truncated channel. Results for a traditional PN channel sounder can be generated by convolving the reported CIR [12] with a PN spectrum [14].

A. Measurement Parameters

TABLE I. Measuremnt Parameters

Center Frequency	2.245 GHz (emulates 2.4 GHz 802.11 b/g/n) 5.412 GHz (emulates 5 GHz 802.11 a/n/ac)
Transmit Power	2.245 GHz – 1.5W 5.400 GHz – 1.25W
Dynamic Range	130 dB insertion loss
Bandwidth	40 MHz (null to null)
PN code length	2047 symbols
Transmit sample rate	Effective symbol rate: 20 MS/s 2x oversampling = 80 MHz sample rate
Receive sample rate	80 MS/s
Effective codeword length	2047 symbols · 2 samples/bit · 2x oversample · 12.5ns/bit = 102.350 µs
Data save rate	Every 200 code words = 20.47 ms Effectively 4.5 MB/sec on disk
Tx antenna	Vertically polarized bi-conical 2.9 dBi max gain @ 2.245 GHz 3.6 dBi max gain @ 5.412 GHz
Rx antenna	Broadband dipole – three orthogonal polarizations -4.2 dBi max gain @ 2.245 GHz -3.5 dBi max gain @ 5.412 GHz
Tx height	5 m
Rx height	1.5 m – 2 m

B. Measurement Path

We present results from a machine shop floor at NIST in Gaithersburg, MD fig. 6. This facility was used as a small-scale version of a commercial industrial facility. It has a large and cluttered ~ 40 x 20 m open area with a ceiling height of 8 m. The walls are concrete block, the floor is reinforced concrete, and the ceiling is steel. There are no exterior windows. Pictures the measurement system are shown in Fig 5.

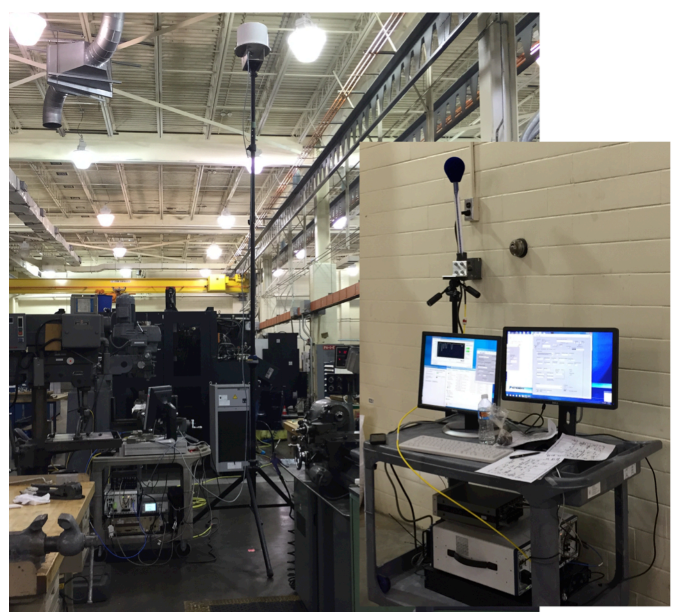

Figure 5. Picture of transmit setup at TX2 (left) and receiver (right).

C. PDP Measuremnt

The PDPs for the transmitter at TX1 and vertically and horizontally polarized receive antennas are calculated using a truncation at 90% of the symbol rate (±~18 MHz channel centered on 2.245 GHz) with no filtering, Fig. 7. The mismatch in polarization results in an approximate 10 dB excess loss compared to the co-polarized case and a lengthened PDP.

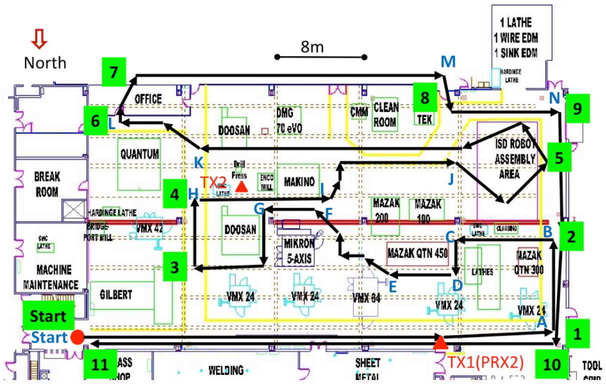

Figure 6. A map of the facility and the measurement path where channel sounding measurements were taken. While code word transmission was continuous, soundings were saved every 20 ms or at ~2 cm intervals.

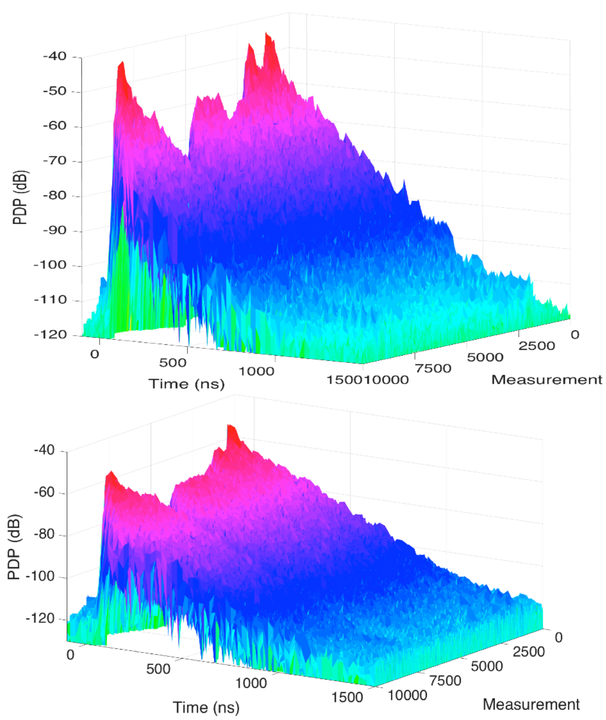

Figure 7. PDP from source location TX1 to a vertically (top) and horizontally (bottom) polarized receive antenna as it transits along the path in Fig. 6. There is a nominal 8-10 dB greater loss for the cross-polarized horizontal case.

D. Path Loss and RMS Delay Spread

The two major parameters generated from the PDP are path loss and RMS delay spread [17]. The path loss is a measure of the propagation loss that needs to be overcome by a combination of antenna gain, transmit power, and receiver sensitivity. The RMS delay spread is a measure of the delay dispersion of the channel (free space= 0 ns) which, in practice, limits the maximum symbol rate in the measured channel due to multi-path induced inter-symbol interference.

The path loss compared to ideal free space for both polarizations is shown in Fig. 8.

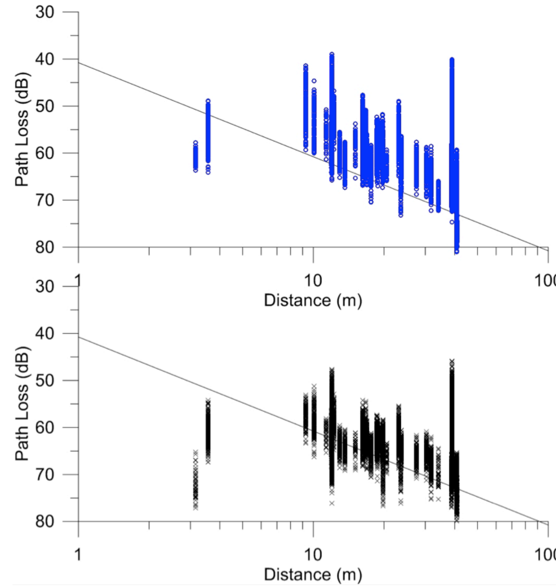

Figure 8. Integrated path loss for both polarizations shown in Fig. 7. The co-polarized transmitter and receiver (vertical/top) show approximately 10 dB less path loss than the cross-polarized (horizontal/bottom) case.

The RMS delay spread with a -20 dB threshold [17] shows similar degradation in the cross-polarized case, Fig. 9.

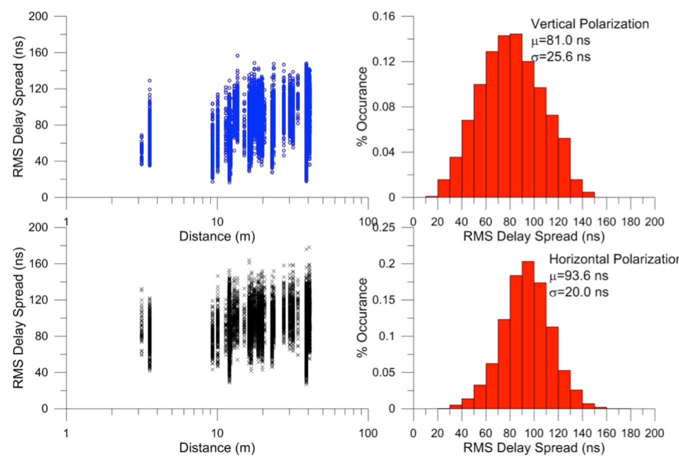

Figure 9. RMS delay spread for two polarizations.

E. Time of Flight and First Arrival.

The channel sounder presented has the ability to measure absolute time between the transmitter and receiver. This can be compared to first peak and maximum peak arrival times, Figs. 10,11. This information can be used to infer line-of-sight suppression, reverberation energy [16], and mixing ratio.

Data in Figs. 10,11 highlight a challenge of wireless communication in an electromagnetically (EM) complex environment. Multi-path propagation can be subject to inter-symbol interference when multi-path is comparable or higher than the direct signal. Proper direction analysis in MIMO systems may reduce errors and improve link quality.

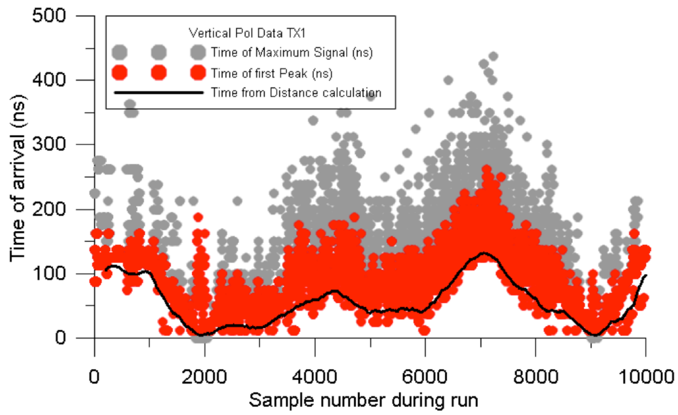

Figure 10. Time of first arrival, time of maximum signal, and distance calculation for the vertically polarized receiver along the path of Fig. 6. The time maximum and first arrival signal do not always correspond to predicted line-of-sight time-of-flight.

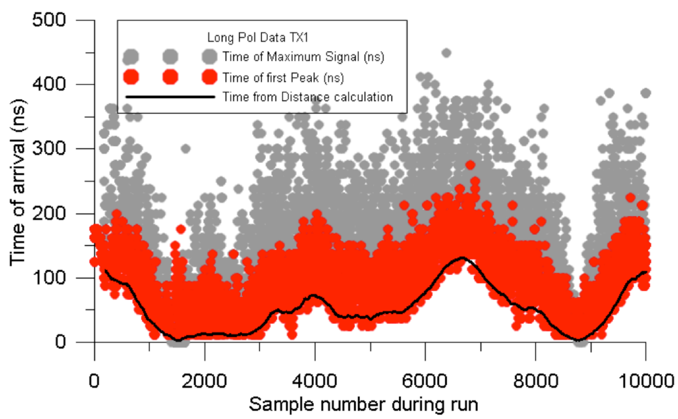

Figure 11. Time of first arrival, time of maximum signal, and distance calculation for the horizontally polarized receiver along the path of Fig. 6.

V. Conclusions

We have presented a 10 MHz-6 GHz channel sounder with absolute time measurement capability. We have covered methods for processing and filtering the data to account for low signal-to-noise caused by band-edge and oversampling. A frequency truncation proposal for determining PDP and derived parameters using frequencies that only have high SNR and has direct correlation to the reported band of significance is presented.

Data for several EM-cluttered facilities were taken and are available for processing by interested parties [12]. Processed data for a small subset were presented to show the results of frequency truncation, antenna polarization, and absolute time capabilities of the new sounder.

References

[1] H.T. Friis, "A note on a simple transmission formula," in Proceedings of the IRE , vol.34, no.5, pp.254-256, May 1946.

[2] J. D Parsons, D. A. Demery, A. M. D. Turkmanil, "Sounding techniques for wideband mobile radio channels: a review," IEE Processings communication, speech and vision., Vol. 138, No. 5, 437-446, 1991.

[3] T. Zwick, T. J. Beukema, Haewoon Nam, "Wideband channel sounder with measurements and model for the 60 GHz indoor radio channel," in Vehicular Technology, IEEE Transactions on , vol.54, no.4, pp.1266-1277, July 2005.

[4] V. Kolmonen, P. Almers, J. Salmi, J. Koivunen, K. Haneda, A. Richter, F. Tufvesson, A.F. Molisch, P. Vainikainen, "A dynamic dual-link wideband MIMO channel sounder for 5.3 GHz," in Instrumentation and Measurement, IEEE Transactions on , vol.59, no.4, pp.873-883, April 2010.

[5] J. Peigang, W. Shaobo; L. Huajia, "An effective solution of wireless channel sounder and its channel modeling application," in Vehicular Technology Conference, 2004. VTC 2004-Spring. 2004 IEEE 59th , vol.1, no., pp.249-253 Vol.1, 17-19 May 2004.

[6] K. Mahler, P. Paschalidis, A. Kortke, M. Peter, W. Keusgen, "Realistic IEEE 802.11p transmission simulations based on channel sounder measurement data," in Vehicular Technology Conference (VTC Fall), 2013 IEEE 78th , vol., no., pp.1-5, 2-5 Sept. 2013.

[7] X. H. Mao, Y. H. Lee, B. C. Ng, "Wideband channel modelling in UHF band for urban area," IEEE International Conference on Wireless Communication Systems, 240-244, Reykjavik, Iceland, October 2008.

[8] T.S. Rappaport, G. R. MacCartney, M.K. Samimi, Shu Sun, "Wideband Millimeter-Wave Propagation Measurements and Channel Models for Future Wireless Communication System Design," in Communications, IEEE Transactions on , vol.63, no.9, pp.3029-3056, Sept. 2015.

[9] Y. Azar, G.N. Wong, K. Wang, R. Mayzus, J.K. Schulz, Hang Zhao, F. Gutierrez, D. Hwang, T.S. Rappaport, "28 GHz propagation measurements for outdoor cellular communications using steerable beam antennas in New York city," in Communications (ICC), 2013 IEEE International Conference on , vol., no., pp.5143-5147, 9-13 June 2013.

[10] N. Yoza, K. Baker, "Narrowband 5 GHz Mobile Channel Characterization," Proc of 37th Meeting of the Antenna and Measurements Techniques Assoc., pp. 335-340, October 2015.

[11] K. Sarabandi, N. Behdad, A. Nashashibi, M. Casciato, L. Pierce, F.Wang, "A measurement system for ultrawide-band communication channel characterization," IEEE Trans. Antennas Propag., vol. 53, pp. 2146-2155, July 2005.

[12] http://www.nist.gov/el/isd/cs/wsie_data.cfm

[13] Richard G. Lyons, Understanding Digital Signal Processing: International Edition, 3rd ed, Prentice Hall, 2011.

[14] R. J. Pirkl and G. D. Durgin, "Revisiting the spread spectrum sliding correlator: why filtering matters," in *IEEE Transactions on Wireless Communications*, vol. 8, no. 7, pp. 3454-3457, July 2009. doi: 10.1109/TWC.2009.081388

[15] P. B. Papazian, J. Choi, J. Senic, P. Jeavons, C. Gentille, N. Golmie, R. Sun, D. Novotny, K.A. Remley, "Calibration of millimeter-wave channel sounders for super-resolution multipath component extraction," *2016 10th European Conference on Antennas and Propagation (EuCAP)*, Davos, 2016, pp. 1-5.

[16] H. Fielitz, K.A. Remley, C.L. Holloway, Qian Zhang, Qiong Wu, D.W. Matolak, "Reverberation-chamber test environment for outdoor urban wireless propagation studies," in Antennas and Wireless Propagation Letters, IEEE , vol.9, no., pp.52-56, 2010.

[17] "Recommendation ITU-R P.1407-5 (09/2013)-Multipath propagation and parameterization of its characteristics," Internatoinal Telecommunications Union, Sept, 2013, https://www.itu.int/rec/R-REC-P.1407-5-201309-I/en.